Published in final edited form as:
J Magn Reson Imaging. 2013 August ; 38(2): 435–440. doi:10.1002/jmri.23988.

RF Field Enhancement with High Dielectric Constant (HDC) Pads in a Receive Array Coil at 3.0 T

Qing X. Yang, PhD[1,2], **Wei Luo, BS**[3], **Sebastian Rupprecht, BE**[1], **Zachary Herse, BS**[1], **Christopher Sica, PhD**[1], **Jianli Wang, MD, PhD**[1], **Zhipeng Cao, BS**[4], **Jeffrey Vesek, BS**[1], **Michael T. Lanagan, PhD**[3], **Giuseppe Carluccio, PhD**[5], **Yeun-Chul Ryu, PhD**[1], and **Christopher M. Collins, PhD**[5]

[1]Department of Radiology The Pennsylvania State University College of Medicine, 500 University Drive, Hershey, PA 17033 USA

[2]Department of Neurosurgery, The Pennsylvania State University College of Medicine, 500 University Drive, Hershey, PA 17033 USA

[3]Department of Engineering Science and Mechanics The Pennsylvania State University, University Park, PA, United States

[4]Department of Bioengineering, The Pennsylvania State University, University Park, PA, United States

[5]Department of Radiology, New York University, NY, United States

Abstract

Purpose—To investigate the use of a new high-dielectric constant (HDC) material for improving SNR and transmission efficiency for clinical MRI applications at 3T with cervical spine imaging.

Materials and Methods—Human subjects were imaged using a commercial cervical spine receive array coil on a clinical system with and without pads containing Barium Titanate beads in deuterium water placed around the neck. Numerical electromagnetic field simulations of the same configuration were also performed.

Results—Experimental and simulated maps of transmit and receive fields showed greater efficiency for imaging the cervical spine when the pads were present. Experimental measurements showed a significant improvement in SNR with the pads present and an average input power reduction of 46%.

Conclusion—Use of HDC material can enhance SNR and transmission efficiency for clinical imaging of the cervical spine at 3.0 T.

Keywords

MRI; B1 field; RF field; SAR; SNR; high permittivity

INTRODUCTION

Recently published experiments at 3.0 T have shown that the placement of high dielectric constant (HDC) pads between the human head and RF coil could significantly improve the

Address correspondence to: Qing X. Yang, Center for NMR Research, NMR/MRI Building, Department of Radiology H066, The Pennsylvania State University College of Medicine, 500 University Drive, Hershey, PA 17033. Phone: (717) 531- 6069. FAX: (717) 531- 8486 qyang@psu.edu.

image signal-to-noise ratio (SNR) while reducing the overall required input RF power (1), thereby reducing SAR deposition to the body. Early experiments using HDC pads for RF field enhancement were performed at 7.0 T, and it was proposed that HDC pads could be utilized as a new method for adjustment of the B_1 field inside the sample to improve the B_1 field inhomogeneity (RF passive shimming) or for local enhancement of the SNR in targeted regions of interest (RF field focusing) (2). The dielectric material used for initial demonstrations at both 7.0 T and 3.0 T was distilled water, which was problematic for practical use because of the overwhelming signal from the pad itself and the potential associated motion artifacts. Recently, a series of investigations using HDC material in form of a slurry with higher permittivity and less signal than water demonstrated more practical methods of utilizing HDC pads for 7T human imaging (3). Among these reports, a detailed study at 7.0 T by Teeuwisse *et al.* showed experimentally that the use of HDC pads neither influenced the coil coupling for an array receive coil nor the B_0 homogeneity in the brain (4). These two issues are critical for a greater application of the HDC pad at 7.0 T where array coils are used almost exclusively and magnetic susceptibility artifacts are pervasive.

Interestingly, the experimental data at 3.0 T suggested that the SNR enhancement with the HDC pad reaches a more extended region from the immediate vicinity of the pad than initially demonstrated at 7.0 T. Thus, HDC pads can be of great value for clinical applications on a 3T system, as it has become the major workhorse for clinical MRI. Considering that most, if not all, of the clinical studies are performed with array receive coils at the present time, it is necessary to demonstrate the utility of the new HDC pads with array coils in a 3.0 T system in order to translate the HDC pad technology for its potential clinical applications. The goal of this study is to demonstrate a new high-dielectric constant (HDC) material for improving SNR and transmission efficiency for clinical MRI applications at 3 T. With cervical spine imaging and computer modeling, we revealed that both the transmission field $|B_1^+|$ from a body coil and reception field $|B_1^-|$ from an array coil can be enhanced locally up to 50% with our HDC material using standard RF coils. Our experimental and computer modeling data demonstrated that the HDC pad can be a simple and low-cost way to improve efficiency of a given RF coil without any hardware or software alterations in a standard clinical system.

MATERIALS AND METHODS

High Dielectric Constant (HDC) Pads

Our HDC pads are made of a mixture of distilled water (dH_2O) or deuterium oxide (D_2O) with barium titanate ($BaTiO_3$) beads. The dielectric constant or permittivity of $BaTiO_3$ varies greatly (5,6) depending on its physical form and processing methods. The permittivity value can be as high as 6000 (6), when it is in solid ceramic form and is drastically reduced in its powder form as a nanometer in size (6). The dielectric constant of the mixture ε_{eff} of $BaTiO_3$ with D_2O or dH_2O water used for the pad is predicted by the permittivity of individual physical phases and the *volume fraction, f*, of each phase of the mixture following a simple mixing rule known as Lichtenecker's logarithmic power law (7):

$$\varepsilon_{\text{eff}}=\varepsilon_{\text{BaTiO}_3}^{\text{f(BaTiO}_3)} \times \varepsilon_{\text{D}_2\text{O}}^{(1-\text{f(BaTiO}_3))}$$

where ε_{BaTiO3} and ε_{D2O} are the permittivity of $BaTiO_3$ and D_2O, and ε_{eff}, is the effective permittivity of the mixture. The volume fraction of barium titanate, f_{BaTiO_3}, is given by:

$$f_{BaTiO_3}=\nu_{BaTiO_3}/\left(\nu_{D_2O}+\nu_{BaTiO_3}\right)$$

Since both f and ε_{BaTiO3} depend on the particle size, ε_{eff} can be varied and maximized by adjusting the particle size of the material. In general, the larger the particle size the greater ε_r is, while the dependence of f on the particle size is determined by the amount of material that can be packed into a given volume with a given particle size (8). For example, the maximum f for the mixture of deuterium water and commercially available $BaTiO_3$ powder with a 400 nanometer particle size (Inframat Advanced Materials) is about 0.45 at 123.25 MHz. The corresponding dielectric constant and conductivity of the mixture is 333 and 0.7 S/m (9). In order to increase the volume fraction for higher dielectric constant of $BaTiO_3$, solid granules of approximately 1 mm diameter were be used (10), which leads to a volume fraction for the mixture with deuterium water up to 0.61. It is 34% higher than that obtained from using barium titanate nanometer powder. The increases in particle size and subsequently volume fraction, *f*, resulted in a dielectric constant of 515 with a conductivity of 0.35 S/m Comparing the beads to the mixture of barium titanate power, the dielectric constant is nearly doubled. In this study, HDC pads were made from granules of barium titanate mixture with D_2O, using durable clear plastic bags with a dimension of 200 mm length, 85 mm width and 10 mm thickness as shown in Figure 1 (11).

Human Imaging

Human spine images were acquired on a Siemens 3T whole body system (Siemens Magnetom TIM Trio, Erlangen, Germany) using a 4-element cervical spine receive array coil. Sagittal and axial cervical spine T_2–weighted images using turbo spin echo (TSE) and T_1-weighted images using gradient recalled echo (GRE) sequences were acquired with and without a collar of HDC pads conformed around the neck using identical imaging parameters. Cervical spine T_2-weighted and T_1-weighted images were acquired with a 3 mm slice thickness, a 30° flip angle (FA), and a 230 mm field of view (FOV). All subjects were initially scanned with HDC pads and then repositioned in the same location and scanned again after the pads were removed. The transmission voltage used of the excitation pulse with and without the HDC pads was adjusted with the Siemens automated calibration routine to ensure that all images were acquired subsequently under these two conditions used correct flip angles as prescribed. The input power and reflected power levels for each excitation were also recorded to ensure that loading of the transmit coil was not significantly changed by HDC pads. Informed consent was acquired from all the human subjects prior to study participation and the imaging protocol approved by our institutional review board.

The image signal-to-noise ratio (SNR) was determined by the ratio of the average signal intensity in the regions of interest (ROI) within the spinal cord and the standard deviation of the image intensity in an ROI in the background of the magnitude images.

B_1^+ mapping was also performed on each subject using the AFI technique (12) with TR_1=20 ms and TR_2=100 ms with and without the HDC pads present. Gradient spoilers (13) were applied along the readout- and slice-select axes with an area of 370 (mT/m) × ms during TR_1 and 1850 (mT/m) × ms during TR_2. The RF spoiling scheme was implemented following Nehrke (13) with the recommended phase shift increment (ϕ) of 129.3°. The acquired 3D FOV was 320 × 260 × 320 mm^3 (z, x, y) with a corresponding matrix size of 128 × 26 × 128, yielding a voxel resolution of 2.5 × 10 × 2.5 mm^3. The excitation pulse utilized was a 300 μs non-selective hard pulse with a nominal flip angle of 60°. For comparison purposes, the experimental $|B_1^+|$ maps with and without HDC pads were normalized to the same transmission voltage.

For calculations of the corresponding receive sensitivities of the four-channel coil, a set of GRE images was acquired with and without the HDC pads with a 150 ms TR, 2° nominal flip angle and identical image resolution as AFI images. Additionally, a “noise scan” for each case was obtained by setting the flip angle to zero. Using the GRE images, an

approximate uniform-receive-sensitivity image was calculated (14,15). The final $|B_1^-|$ map was obtained subsequently by dividing the sum of square of the GRE images from all the channels with the uniform-receive-sensitivity image to remove the anatomical contributions. To compare the receive sensitivity enhancement by the HDC pads, the $|B_1^-|$ maps with and without the HDC pad collar were normalized with the standard deviation of the noise scan in each case.

Computer modeling

To further demonstrate the effect of the HDC pads on the receive array coil, a numerical model with finite difference time domain (FDTD) method was used to calculate the RF field distribution in the human body in a coil model shown in Figure 2. All the RF field calculations were performed with XFDTD software (Remcom, Inc., State College, PA), and post-processing of the simulation results was performed with in-house software in MATLAB (The Mathworks, Inc., Natick, MA). The calculation was performed with −35dB convergence to ensure that the steady state was reached. A Liao boundary condition was used for the outer boundary truncation of the grid. The RF coil models were modeled using similar geometry and dimension of the coil used in experiment. A unit current source at 123.26 MHz having appropriate phase was assigned to each coil element at a port on a capacitor for generation of the quadrature-driven mode. The cervical spine coil model consists of a 4-loop array with unit current sources placed at the capacitors. The human head model (“Duke”) used for the FDTD calculation included sixteen types of tissue and the corresponding electric properties at 123.26 MHz were derived by linear interpolation from experimentally measured values by Gabriel, et al (16). The human model at 5-mm3 resolution was placed at the isocenter of the birdcage coil as shown in Figure 2 (16,17). The 10 mm-thick dielectric pads were placed around the neck extended throughout the cervical spine with a dielectric constant of 515 and conductivity of 0.35 S/m used for the experiment (9). The transmit field map, $|B_1^+|$, was generated from the birdcage volume coil and receive sensitivity map, $|B_1^-|$, was generated by sum of square of $|B_1^-|$ of each individual loop in the receive array (18) in the simulation.

RESULTS

Figure 3 shows the experimental and calculated RF transmission field $|B_1^+|$ maps of the body coil and reception field $|B_1^-|$ maps of the 4-element receive array coil with and without the HDC pads. Both experimental and calculated $|B_1^+|$ and $|B_1^-|$ maps exhibited similar patterns and trends of enhancement after placement of HDC pads. Since the transmission field was generated by a body volume coil, $|B_1^+|$ was enhanced (20–50%) in the cervical spinal region, particularly, near the HDC pads and was reduced in other areas such as the head and face. Consequentially, the $|B_1^+|$ field became less homogeneous, i.e., the enhancements appeared less prominent in the throat area than in the back of the neck. For the experimental reception field, the 30–40% enhancement with the HDC pads appeared more uniform throughout the neck region enclosed by the receive array coil and the HDC pads. The rectangular shaped ROI in the $|B_1^-|$ map shows an example area corresponding to the spinal cord region where the SNR was assessed in Figure 4. The average $|B_1^-|$ enhancement in the ROI was 29±5 % (Mean ± SD).

The computer modeling results shown in Figure 3 demonstrated a clear trend of enhancement by the HDC pad for both the transmission field by the body coil and the reception field by the cervical spine array coil. As exhibited experimentally, the transmission field enhancement led to a reduction in the RF power required for excitation

while the reception field $\left(|B_1^-|\right)$ enhancement directly resulted in a SNR increase. Notice also that the patterns of enhancements of the experimental and calculated B_1 maps are not identical. This disagreement is most likely associated with the differences in geometries of the HDC pads and human subject between the experimental and computer modeling.

Figure 4 shows sagittal and axial T_2- and T_1-weighted images from the cervical spine acquired using standard clinical protocols with and without HDC pads on the same subject. The signal intensities are visibly increased with the HDC pads, particularly in the posterior aspect of the neck. As shown in the corresponding axial images, signal enhancement can be seen over the entire axial slice except in the throat area. The cervical spinal cord shows increased signal intensity and image homogeneity from the medullary-cervical to the cervicothoracic junctions. The cervical spinal cord and its associated spinal column exhibit greater image clarity with the introduction of the HDC pads. Note the improved contrast in T_1-weighted images of the CSF-cord junction. The image enhancements in terms of clarity and SNR without degradation in homogeneity with the HDC pads suggest many potential clinical applications in spinal pathology.

As indicated in Table 1, the SNR in the T2-weighted images was improved by 29–45% in the spinal cord across all seven vertebrae with the pad, while contrast between CSF and spinal cord remained the same. The signal intensity appeared to be much stronger closer to the surface near the pad. The SNR enhancement here is consistent with the experimental $|B_1^-|$ maps in Figure 3, where the coil sensitivity, $|B_1^-|$, is increased by 29 ± 5 % with the HDC pads within the ROI corresponding to the spinal cord regions in Figure 4. Deeper into the neck, the SNR enhancement appeared reduced. The SNR increase in the discs between vertebral bodies was calculated to be as much as 20%.

Before images were acquired under each condition, RF power calibrations were performed. Placement of the HDC pads around the neck resulted in a 46.28 ±14.55 % (Mean ± SD) average transmission power reduction by the body coil. For a given sample load, reduction of transmission power of an imaging protocol can be translated into SAR reduction, which, in turn, can lead to an increase of throughput or a larger volume coverage.

Discussion

For human imaging of the spine and extremities, specialized local reception coils are commonly used to improve the image quality while reducing imaging times. In these studies, a significant amount of RF power is transmitted into the whole body while imaging only a small part of it. In this case, the local imaging protocols are subject to whole-body SAR limitations, which, in turn, reduce the throughput. As demonstrated, by strategic placement of the HDC pads next to or around regions or organs of interest, RF transmission power can be reduced by as much as 50%. With SNR enhancement and SAR reduction, more rapid imaging with improved quality can be achieved simply by placement of the HDC pad. In our experiment, we used a cervical spine coil to demonstrate the effectiveness of HDC pad with receive array coils. Evidently, the HDC pad can be used for all other specialized local array coils such as knee, shoulder, foot and wrist where high spatial image resolution is desirable. The enhanced SNR with the HDC pad can be used for higher spatial resolution or higher throughput in SNR-limited scans requiring multiple averages and SAR-limited cases. In addition, these significant improvements were achieved without any hardware and software alterations. Thus, the experimental results presented here open up possibilities for broad clinical applications of HDC pads on 3 T systems, and these applications can be immediately implemented on the most standard clinical MRI systems.

The computer modeling results shown in Figure 3 are consistent with our experimental data and illustrate that the HDC pads increased both the transmission field by the body coil and reception field by the cervical spine coil in the region near the pads. Theoretically, the transmission field enhancement would lead to a reduction in the RF power required for excitations, while enhancement of the reception field would directly result in a SNR increase. From an RF coil engineering perspective, undoubtedly, these results can be further improved with systematic optimizations in the pad geometry and electric properties for specific RF coils. For example, the addition of a certain amount of HDC material into a RF transmission coil may vary the loading of the coil, and to some extent, change the tuning and matching conditions, which could change the required RF power. In all of our human studies, the transmitted and reflected power levels for each imaging sequence were recorded. We observed the overall power reduction of both transmitted and reflected power after placement of HDC pads but no significant changes in the ratio of the two were observed. Thus, the potential contribution of loading change to the reduction of the transmission power by the HDC pad is insignificant. Correspondingly, for array receive coils, loading with HDC could potentially alter the coupling characteristics of coil elements. Similar to the transmission field, however, our data with the cervical spine coil indicated that the HDC pads have no measurable effect on coil element coupling. These results are consistent with a previous study at 7.0 T (4). Nevertheless, it is highly likely that the results presented here were obtained in far from optimized conditions. Therefore, for optimal utilization of HDC pads for RF field enhancement, it would be ideal to design future transmission and reception coils with consideration of HDC pads around human subjects.

The SNR increases and RF power reductions achieved in this study were realized with a dielectric constant more than six-fold greater than that of dH2O used in the previous study at 3T. We expect that even greater improvements can be achieved with new HDC material. In our previous work, we theorized that B1 enhancement by the HDC pads was produced by the constructive contribution from the displacement current induced inside the HDC pads as a secondary field source (19). Thus, in general, one may expect that the higher the dielectric constant of the material, the stronger of the effect of B_1 enhancement. However, caution must be given that the geometric configurations of the HDC pad are also important factors to the effect. One extreme example would be that standing waves could be formed inside the HDC pad if the dimension of the pad would reach to a quarter of the wavelength of the RF field inside the pad in a given static field strength. If this would occur, the RF field near the pad could be destructive, such that the B_1 field near the HDC pad would be reduced and become extremely inhomogeneous. We expect that greater improvements can be achieved with further investigations by optimizing dielectric constant values and geometries of the pads in conjunction with the RF coil at given static field strength. In addition, we observed an appreciable amount of variation in SNR improvement and RF power reduction among our human subjects. Although this commonly occurs for all the clinical systems in the case without using HDC pads, more careful computer modeling studies should be carried out to evaluate the couplings between the human body and the HDC pad with various coil configurations and at different field strengths. With further development, use of HDC pads may provide a simple, effective and low-cost method for improving quality and safety of MRI in a variety of applications.

From an RF engineering point of view, the HDC pads presented here is only one potential application of HDC material to enhance and manipulate the RF field for achieving desirable imaging results. As demonstrated in the $|B_1^+|$ and $|B_1^-|$ maps, HDC material could significantly alter the B1 field of both transmission and reception fields and their spatial distribution inside the human body. It is conceivable that rigid or flexible solid materials could be directly incorporated into RF coil design and patient bed manufacturing to achieve the

desired result. Thus, our data suggest that HDC material has a great potential for RF field engineering.

In both this work and a previous study (1) showing significant overall improvement in SNR and reduction of SAR when the region of interest was surrounded by HDC material, the region of interest was smaller than either the transmit or receive coils. Further dedicated studies will be required to determine effects on SNR for arrays of surface coils that are smaller when compared to the region of interest and HDC pad.

In conclusion, we have developed an HDC pad with an increased permittivity increased up to 515 at 3.0 T to replace the previous water-based pad. We demonstrated that proper placement of dielectric material such as our HDC pad could enhance both transmission and reception fields, resulting in reduced RF transmission power and improved image SNR throughout the cervical spine. With further exploration and development, utilization of dielectric material in RF field engineering for improving quality and safety of MRI in a variety of applications is clearly warranted.

Acknowledgments

Authors are thankful to Mark A. Griswold Ph.D. from Case Western University for helpful discussions and sharing the code for receive sensitivity mapping.

Grant Support: Funding has been provided in part through NIH R01 EB000454, NIH R01 AG02771 and the Pennsylvania Department of Health.

REFERENCES

1. Yang QX, Wang J, Collins CM, Wang C, Smith MB. Reducing SAR and enhancing cerebral signal-to-noise ratio with high permittivity padding at 3 T. Magn Reson Med. 2011; 65(2):358–362. [PubMed: 21264928]
2. Yang QX, Mao W, Wang J, et al. Manipulation of image intensity distribution at 7.0 T: passive RF shimming and focusing with dielectric materials. J Magn Reson Imaging. 2006; 24(1):197–202. [PubMed: 16755543]
3. Haines K, Smith NB, Webb AG. New high dielectric constant materials for tailoring the B1+ distribution at high magnetic fields. J Magn Reson. 2010; 203(2):323–327. [PubMed: 20122862]
4. Teeuwisse WM, Brink WM, Haines KN, Webb AG. Simulations of high permittivity materials for 7 T neuroimaging and evaluation of a new barium titanate-based dielectric. Magn Reson Med. 2012; 67(4):912–918. [PubMed: 22287360]
5. McNeal MP, Jang S-J, Newnham RE. The effect of grain and particle size on the microwave properties of barium titanate $BaTiO_3$. J Appl Phys. 1997; 83(6):3288.
6. Petrovsky V, Petrovsky T, Kamlapurkar S, Dogan F. Dielectric Constant of Barium Titanate Powders Near Curie Temperature. J Am Ceram Soc. 2008; 91(11):3590–3592.
7. Simpkin R. Derivation of Lichtenecker's Logarithmic Mixture Formula From Maxwell's Equations. Ieee T Microw Theory. 2010; 58(3):545–550.
8. McGeary RK. Mechanical Packing of Spherical Particles. J Am Ceram Soc. 1961; 44(10):513–522.
9. Luo, W.; Ryu, YC.; Oh, S., et al. Improved material for passive RF shimming with high dielectric pads. Proceedings of the 20th Annual Meeting of ISMRM; Melbourne. 2012. p. 2700
10. Yang, QX.; Herse, ZG.; Ketterman, M., et al. Enhancement of RF field by high dielectric constant pad at 3T: Cervical Spine Imaging. Proceedings of the 19th Annual Meeting of ISMRM; Montréal. 2011. p. 621
11. Haines, K.; Neuberger, T.; Lanagan, M.; Semouchkina, E.; Webb, AG. Calcium titanite based ceramic resonators for high field magnetic resonance. Proceedings of the 17th Annual Meeting of ISMRM; Honolulu. 2009. p. 502

12. Yarnykh VL. Actual flip-angle imaging in the pulsed steady state: a method for rapid three-dimensional mapping of the transmitted radiofrequency field. Magn Reson Med. 2007; 57(1):192–200. [PubMed: 17191242]

13. Nehrke K. On the steady-state properties of actual flip angle imaging (AFI). Magn Reson Med. 2009; 61(1):84–92. [PubMed: 19097210]

14. Walsh DO, Gmitro AF, Marcellin MW. Adaptive reconstruction of phased array MR imagery. Magn Reson Med. 2000; 43(5):682–690. [PubMed: 10800033]

15. Griswold, M.; Walsh, D.; Heidemann, R.; Haase, A.; Jakob, P. The Use of an Adaptive Reconstruction for Array Coil Sensitivity Mapping and Intensity Normalization. Proceedings of the 10th Annual Meeting of ISMRM; Honolulu. 2002. p. 2410

16. Gabriel S, Lau RW, Gabriel C. The dielectric properties of biological tissues: II. Measurements in the frequency range 10 Hz to 20 GHz. Phys Med Biol. 1996; 41(11):2251–2269. [PubMed: 8938025]

17. Christ A, Kainz W, Hahn EG, et al. The Virtual Family—development of surface-based anatomical models of two adults and two children for dosimetric simulations. Phys Med Biol. 2010; 55:N23–N38. [PubMed: 20019402]

18. Roemer PB, Edelstein WA, Hayes CE, Souza SP, Mueller OM. The NMR phased array. Magn Reson Med. 1990; 16(2):192–225. [PubMed: 2266841]

19. Yang QX, Wang JL, Wang JH, Collins CM, Wang CS, Smith MB. Reducing SAR and Enhancing Cerebral Signal-to-Noise Ratio with High Permittivity Padding at 3 T. Magnet Reson Med. 2011; 65(2):358–362.

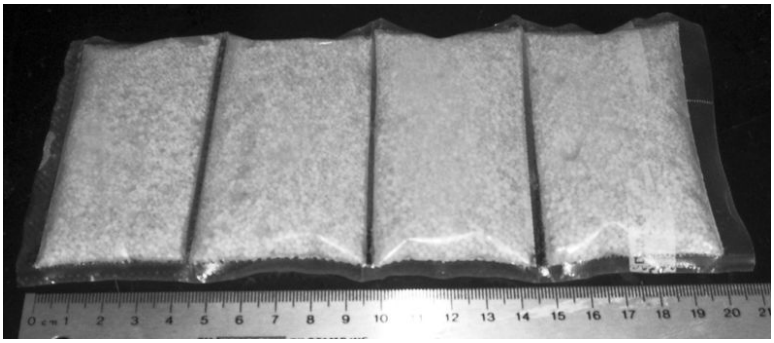

Figure 1.
The HDC pad as used experimentally with 4 compartments, each filled with 90g $BaTiO_3$ granules mixed with and 15mL D_20.

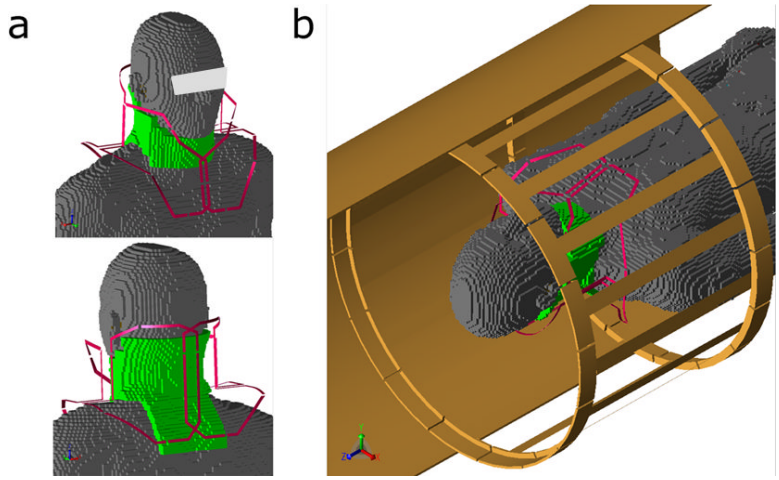

Figure 2.
Computer model of the coil-human body configuration for RF field calculation. a) The HDC pad (green) is placed around the neck and over the back of the human model inside the 4-element receive coil (red). b) The entire computer modeling setup with body coil and part of shield (brown).

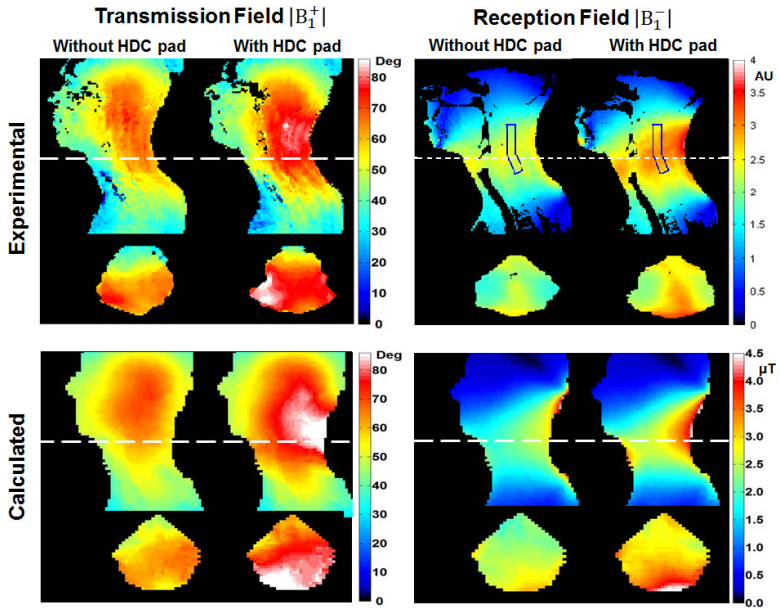

Figure 3.

The experimentally measured and numerically calculated $|B_1^+|$ and $|B_1^-|$ fields with and without the HDC pads in sagittal and axial views. For comparison purposes the experimental $|B_1^+|$ maps are normalized with the transmission voltage while the $|B_1^-|$ maps are normalized by the standard deviation of the "noise scan". The calculated $|B_1^+|$ and $|B_1^-|$ maps are normalized by the input current in the conductor elements in the coil model. To correlate the $|B_1^-|$ enhancement with SNR in the corresponding region in Fig. 4, an ROI is selected in the spinal cord region. The average $|B_1^-|$ enhancement in the ROI is 29±5% (Mean ± SD).

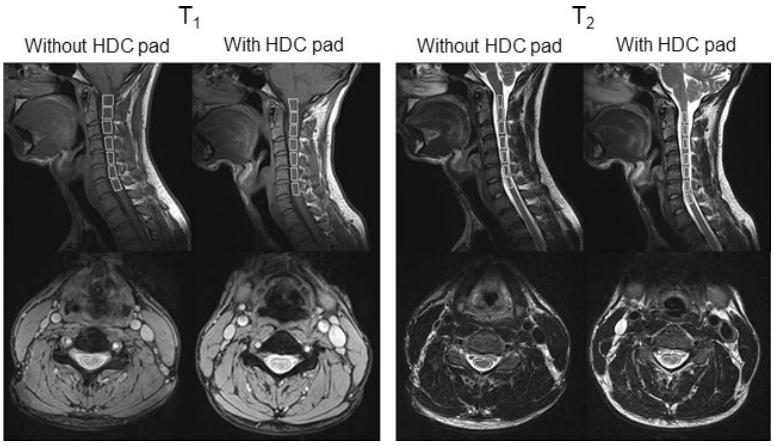

Figure 4.
Cervical spine GRE T_1- and TSE T_2- weighted sagittal and axial images. Seven ROIs within the spinal cord are shown and the corresponding SNRs are listed in Table 1.

Table 1

The SNR increases averaged over 4 subjects in 7 ROIs along the spinal cord at the 7 upper cervical spine vertebrae in TSE T_2- and GRE T_1-weighted images.

ROI	SNR increase T_2 image [%]±SD	SNR increase T_1 image [%]±SD
C1 (medulla)	41.96 ±7.34	34.7 ±5.46
C2	45.23 ±4.83	42.11 ±5.44
C3	40.31 ±6.05	39.63 ±8.1
C4	38.09 ±14.72	35.56 ±12.53
C5	36.99 ±10.28	30.01 ±10.49
C6	33.11 ±6.53	26.63 ±11.72
C7	28.58 ±9.43	22.02 ±9.04
Average Increase	37.75 ±5.16	32.95 ±6.62